Communications of BAO, Vol. 73, Issue 2, 2026, pp. 227–248

Relationship between optical stellar flares and infrared variability: I. Cross-matching the TESS, Kepler and K2 flare catalogues with WISE/NEOWISE single-exposure photometry

A. Akopian*, G. Kostandyan, and D. Baghdasaryan

Byurakan Astrophysical Observatory (BAO), NAS RA, Byurakan 0213, Aragatsotn Province, Armenia

Abstract

Nearly everything that space photometry has taught us about flares of late-type stars has been obtained in the visible range. We present a program and first results of a systematic cross-match of the TESS (three samples, about 150 000 events on ∼15 000 stars), Kepler (79 000 events, 1742 stars) and K2 (2600 events in the Pleiades, Hyades and Praesepe) flare catalogues with the infrared photometry of the WISE/NEOWISE surveys (3.4 and 4.6 μm, 2014–2024). The observing geometry of TESS and WISE drastically reduces the area of the sky where simultaneous observations are possible, although each telescope alone covers the entire sky. For every star, we determine the quiescent infrared level from hundreds of exposures, measure the deviations from it around each flare, and select events by shape and quality. Preliminary 95% upper limits on the flare-averaged infrared brightening within ±0.2 d of the flare peak at 3.4 μm are 4.9 mmag (Kepler × AllWISE, 129 flares) and 0.96 mmag (TESS × NEOWISE, 796 flares); a slow, brightness-dependent drift of the NEOWISE photometry, which imitates a mean dimming of several mmag at the flare times if the quiescent level is taken over the whole mission, is identified and allowed for. In addition, we identify stars for which NEOWISE, at its 95-minute cadence, reproduces the eclipses and rotational modulation seen by TESS (correlation up to 0.98), as well as spurious catalogue flares located at eclipse edges.

Keywords: *stars: flare — stars: activity — infrared: stars — methods: data analysis — surveys*

1 Introduction

The study of non-stationary stars, and of flare stars in particular, is one of the principal research directions of the Byurakan Observatory, which celebrates its eightieth anniversary in 2026. As early as 1954 Ambartsumian drew attention to the non-thermal continuous emission of young stars — members of stellar associations, T Tauri and UV Ceti stars — and to the physical similarity of their radiation, which pointed to an evolutionary link between these classes (Ambartsumian, 1954; Haro, 1957). A statistical analysis of flares in the Pleiades showed that in a cluster of that age, nearly all red dwarfs fainter than a certain absolute magnitude must be flare stars, and hence that the flare stage is a regular phase in the evolution of red dwarfs (Ambartsumian, 1969; Ambartsumyan et al., 1970).

This conclusion initiated an international programme of photographic monitoring of clusters and associations — the Pleiades, Orion, Praesepe, the Hyades, NGC 7000 — with the wide-field Schmidt cameras of Byurakan, Asiago, Tonantzintla, Abastumani, Konkoly and Rozhen. The chain method (several consecutive images of a star on one plate, with exposures of up to 5–10 min) led to the discovery of hundreds of new flare stars and to flare statistics in systems of different ages, while photoelectric time series of UV Ceti stars in the solar neighbourhood yielded a Poissonian description of the flare sequence (Oskanian & Terebizh, 1971). The statistical methods developed in Byurakan for estimating the total number of flare stars, the flare frequency and its evolutionary changes are summarised in the review by Akopian (2021).

Regular observations of flare-star systems ceased in the early 1980s, and over the following two decades, flare statistics grew slowly. The situation was changed by space photometric surveys.

*Corresponding author: aakopian57@gmail.com

Photographic monitoring of the 1970s–1980s detected a flare as a brightening of at least one image in the chain: the detection threshold was 0.5–1.0 mag in the UBV bands, the time resolution was the 5–10 min exposure, and the coverage was limited to the clear nights of a single season, so the completeness of the sample, the flare frequency, and the energy distribution had to be recovered statistically, with corrections for gaps and for the detection threshold; photoelectric photometry provided a precision of hundredths of a magnitude and a time resolution of seconds, but only for a few stars per night. Kepler, K2, and TESS removed both limitations: continuous time series with cadences from 20 s to 30 min and a precision of a fraction of a percent for tens and hundreds of thousands of stars provide the complete light curve of every flare — the times of onset, peak, and end, the amplitude, and the equivalent duration — while the number of events per star reaches hundreds, which makes it possible to study the flare statistics of an individual star rather than of a system as a whole. The K2 fields, moreover, included the Pleiades, the Hyades and Praesepe — the systems where ground-based monitoring began.

Flares are the most readily observable manifestation of the activity of late-type stars (Benz & Güdel, 2010; Gershberg, 2005), and the Kepler (Borucki et al., 2010), K2 (Howell et al., 2014) and TESS (Ricker et al., 2015) space telescopes have turned them into a subject of mass statistical studies: the catalogues contain hundreds of thousands of events (Davenport, 2016; Feinstein et al., 2024; Günther et al., 2020; Ilin et al., 2019, 2021; Seli et al., 2025; Shibayama et al., 2013; Walkowicz et al., 2011; Yang & Liu, 2019; Yudovich et al., 2025). A uniform reprocessing of the TESS light curves with the TOFFEE algorithm (Pratt et al., 2026) has produced homogeneous samples with common quality criteria. These data have been used to study the energy and frequency distributions of flares (Davenport et al., 2019; Hawley et al., 2014; Maehara et al., 2012), their dependence on age and rotation (Feinstein et al., 2024; Ilin et al., 2019, 2021), flare morphology (Davenport et al., 2014; Seli et al., 2025; Yudovich et al., 2025) and other properties. On the basis of the Kepler catalogue, the periodic flare-frequency function of the most active flare stars and the starspot coverage derived from it (Akopian, 2024), as well as the fractional-Poisson structure of the inter-flare intervals and the distribution of active-region flare rates within individual stars (Akopian & Sargsyan, 2026), have also been studied.

The photometry of the space telescopes has inherited a limitation of the earlier monitoring programmes: it was carried out in a single broad band of the visible range (Kepler: 420–900 nm, TESS: 600–1000 nm). The colour and temperature of a flare cannot be derived from these data, whereas the UBV photometry of the 1970s provided at least the colour indices of a flare. The spectral energy distribution of a flare — a hot continuum with a temperature of about 10^4 K and hydrogen lines (Hawley & Fisher, 1992; Kowalski, 2024; Kowalski et al., 2013, 2016) — has been measured for only a few dozen events, almost exclusively in the ultraviolet, X-ray and visible ranges (Davenport et al., 2012; Feinstein et al., 2022; Jackman et al., 2023; Loyd et al., 2018; Osten & Wolk, 2015; Osten et al., 2005; Pye et al., 2015). In the near infrared, observations simultaneous with the optical ones are few and have revealed only hydrogen and helium emission lines without any enhancement of the continuum: in the J, H and K_s bands it changes by no more than 5–8 mmag (Schmidt et al., 2012; Tofflemire et al., 2012); in JWST spectra the response has been studied for isolated events (Howard et al., 2023); at 3–5 μm simultaneous observations are absent. At the same time, the diversity of flare shapes calls for multicolour data (Seli et al., 2025), and Yudovich et al. (2025) attribute the secondary maxima ("bumps") on the decay branch to a change in the temperature of the emitting region. The possible manifestations of a flare at 3–5 μm — the long-wavelength part of its own continuum, the reprocessing of its energy by circumstellar matter, and a dimming or brightening of the star before and after the flare — are considered quantitatively in Section 6; the search in the present work is not restricted to a response of a particular sign or direction in time.

Such a search has become possible owing to the NEOWISE survey (Mainzer et al., 2011, 2014): from December 2013 to July 2024 (referred to below as 2014–2024) the WISE space telescope (Wright et al., 2010) surveyed the entire sky every six months in the W1 (3.4 μm) and W2 (4.6 μm) bands, so that for every star a single observing series (visit) accumulates 10–20 exposures, and the whole survey hundreds of exposures, spaced by about 95 min; these are available in the IRSA archive with a precision of about 0.02 mag for stars of 11–13 mag. For the Kepler field there is, in addition, the multi-epoch photometry of the AllWISE release (two observing series in 2010, the first of them in the cryogenic phase with the W3 and W4 bands; Cutri et al. 2013). The flare surveys and NEOWISE overlap in time by ten years, but, as shown below, the pointing geometry makes strictly simultaneous observations rare.

In the present work, we describe a program that cross-matches the TESS, Kepler, and K2 flare catalogues with the individual NEOWISE and AllWISE measurements. The preliminary results outline a set of problems that will be examined in more detail in the near future, among them: (1) the search for a re-

doi: https://doi.org/10.52526/25792776-26.73.2-227

sponse at 3–5 μm, averaged over thousands of events during the first day after a flare; (2) the identification of individual events — possible evidence of a connection between a flare and the infrared emission — in which WISE exposures fall within minutes or hours before and after the flare; (3) by-products: the infrared periodicity of stars and the control of spurious flares in the catalogues.

2 Data

2.1 Flare catalogues

Five catalogues are used (Table 1). Three TESS samples with 2-min cadence — members of young groups and clusters (Feinstein et al., 2024), the most active F–M stars (the sample of Crowley et al. 2022 analysed by Yudovich et al. 2025) and all 2-min-cadence stars, mostly M dwarfs within 200 pc (Seli et al., 2025) — are taken from the uniform reprocessing with the TOFFEE algorithm (Pratt et al., 2026), which provides for every event the times of onset, peak, and end, the amplitude, the equivalent duration, the number of points, and the ratio of the amplitude to the scatter. The quality selection is identical for all three: at least five points per event and an amplitude of at least five times the scatter of the light curve; for complex events, only the primary peak is kept. The Kepler catalogue comprises the flares of Yang & Liu (2019) for the 1742 stars that have AllWISE multi-epoch photometry; the peak times, which the catalogue does not give, were recovered from the light curves. The K2 catalogue comprises the flares of open-cluster members from Ilin et al. (2021); Campaigns 4 (Pleiades, Hyades) and 5 (Praesepe), which fall within the NEOWISE operation, are used. The light curves used for recovering the peak times and for the figures are the SPOC PDCSAP fluxes at 2-min cadence for TESS, the PDCSAP fluxes (Smith et al., 2012; Stumpe et al., 2012) for Kepler, and the EVEREST product (Luger et al., 2016) for K2; in the crowded Pleiades field, the wider EVEREST apertures give flare amplitudes 25–30% smaller than the PDCSAP ones, which does not affect the peak times or the limits derived below.

Table 1: Flare catalogues. "Used": events of stars with at least 15 WISE measurements outside flares, sufficient for the quiescent infrared level to be determined (Section 3).

Catalogue	Sample	Cadence	Events in source	After selection: events / stars	Used: events / stars
Feinstein et al. (2024), TESS	members of 26 groups and clusters, 4–300 Myr, $T_{\rm eff} \leq 5930$ K	2 min	19 422	13 011 / 2043	11 744 / 1887
Yudovich et al. (2025), TESS	234 most active F–M stars	2 min	14 541	9 964 / 233	9 754 / 225
Seli et al. (2025), TESS	all 2-min-cadence stars; M dwarfs within 200 pc	2 min	187 445	132 383 / 13 298	122 958 / 12 245
Yang & Liu (2019), Kepler	Kepler-field stars with AllWISE photometry	30 min	—	— / 1742	79 287 / 1742
Ilin et al. (2021), K2	Pleiades, Hyades (C4), Praesepe (C5)	30 min	3 844 (5 clusters)	2 592 / 861	2 544 / 841

2.2 Infrared data

For every star all individual measurements of the NEOWISE-R Single Exposure (L1b) Source Table within a 3″ radius were retrieved from the IRSA archive: the exposure time, the W1 and W2 magnitudes with their errors, and the frame-quality indicators. The NEOWISE times (MJD, UTC) are compared directly with the barycentric times of the flare catalogues: the difference between the two scales (the light-travel time across the Earth's orbit, below 8.3 min, and the 69-s offset between TDB and UTC) is negligible on the scale of the intervals used below and is evaluated separately for individual events within minutes of a flare. For the TESS stars the measurement table contains 6.05 million measurements of 14 425 stars over 2014–2024, on average 420 (median 322) epochs per star; the median error of a single epoch is 0.017 mag in W1 and 0.016 mag in W2. The measurements are grouped into observing series — sequences of exposures spaced by about 95 min over 1–2 d (longer near the ecliptic poles) and repeated every six months. For the Kepler stars the AllWISE Multiepoch Photometry table (Cutri et al., 2013) was used: the series of April–May and October–November 2010, the first of them with the *W3* (12 μm) and *W4* (22 μm) bands of

doi: https://doi.org/10.52526/25792776-26.73.2-227

the cryogenic phase. The light curves for the combined figures are taken from the MAST archive: TESS (PDCSAP, SPOC and TESS-SPOC), Kepler (PDCSAP) and K2 (EVEREST, K2SFF). Coordinates and proper motions are taken from the TIC (Stassun et al., 2019) and EPIC, i.e. ultimately from Gaia (Gaia Collaboration et al., 2023).

3 The program

3.1 Structure

The program is written in Python and is the same for all catalogues: only the reading modules, which bring a catalogue and its light curves to a common format, differ. The processing proceeds in steps, each of which can be repeated separately:

1. **Catalogue reading**: star identifiers, times of onset, peak and end (in MJD), amplitude and equivalent duration; for Kepler and K2 the peak time is recovered from the light curve between the onset and the end of the event.
2. **Quality selection of events** (Section 2).
3. **Completion of the NEOWISE measurement sample**: a cone search of 3″ radius in the IRSA archive for every star not yet present in the measurement table; stars without measurements are placed on a separate list and are not queried again; for stars with large proper motion the identification follows the star's track (Section 3.3).
4. **Quiescent level and deviations** (Section 3.2).
5. **Simultaneity summary**: for every flare, the time to the nearest clean WISE exposure before and after the peak; tables by interval and by ecliptic latitude (Section 4).
6. **Combined figures**: for every WISE observing series containing a flare with an exposure in the search interval — the light curve, the variations of W1, W2 and W2−W1 with the intervals marked, and the deviations as a function of time after the peak for all flares of the series (Figs. A1–A4; a simplified two-panel form is used in Figs. 1 and 5).
7. **Star classification**: from the figures a star is classified as flaring, eclipsing, rotational, pulsating or mixed; on a repeated run classified stars are skipped.
8. **Cleaned catalogue**: events of non-flare shape (ratio of decay to rise duration below 1.5, or rise longer than 60 min) and events of stars classified as eclipsing or pulsating are excluded.
9. **Averaging and upper limits** (Section 5).
10. **Verification of individual events**: all frames of the observing series with their full quality indicators, L1b image cut-outs from the archive, Gaia neighbours, and the position of the exposure on the light curve.

3.2 Quiescent infrared level, deviations and time intervals

Selection of measurements. An exposure is considered clean if its archive quality indicators satisfy the adopted thresholds: no image artefacts (`cc_flags` = 0000), frame quality `qual_frame` ≥ 5, a non-zero distance from the South Atlantic Anomaly and no moonlight contamination; for the verification of individual events the stricter `qual_frame` = 10 and `qi_fact` = 1 are required, since a single exposure, unlike an average over thousands, is not protected by the statistics; for AllWISE, where the frame-quality indicator is not published, the criterion is composed of the same conditions with the additional requirement rchi2 < 10 on the quality of the profile-fit photometry. Of the measurements within the 3″ radius — half the width of the WISE point-spread function in W1 — those clustering around the source nearest to the catalogue position are kept; for stars with large proper motion the centre of the circle moves with the star (Section 3.3).

Quiescent level. The quiescent level of a star in each band and in the colour W2−W1 is the median of the clean exposures outside the vicinity of all its flares (from −0.85 to +2.1 d of a peak, somewhat wider

doi: https://doi.org/10.52526/25792776-26.73.2-227

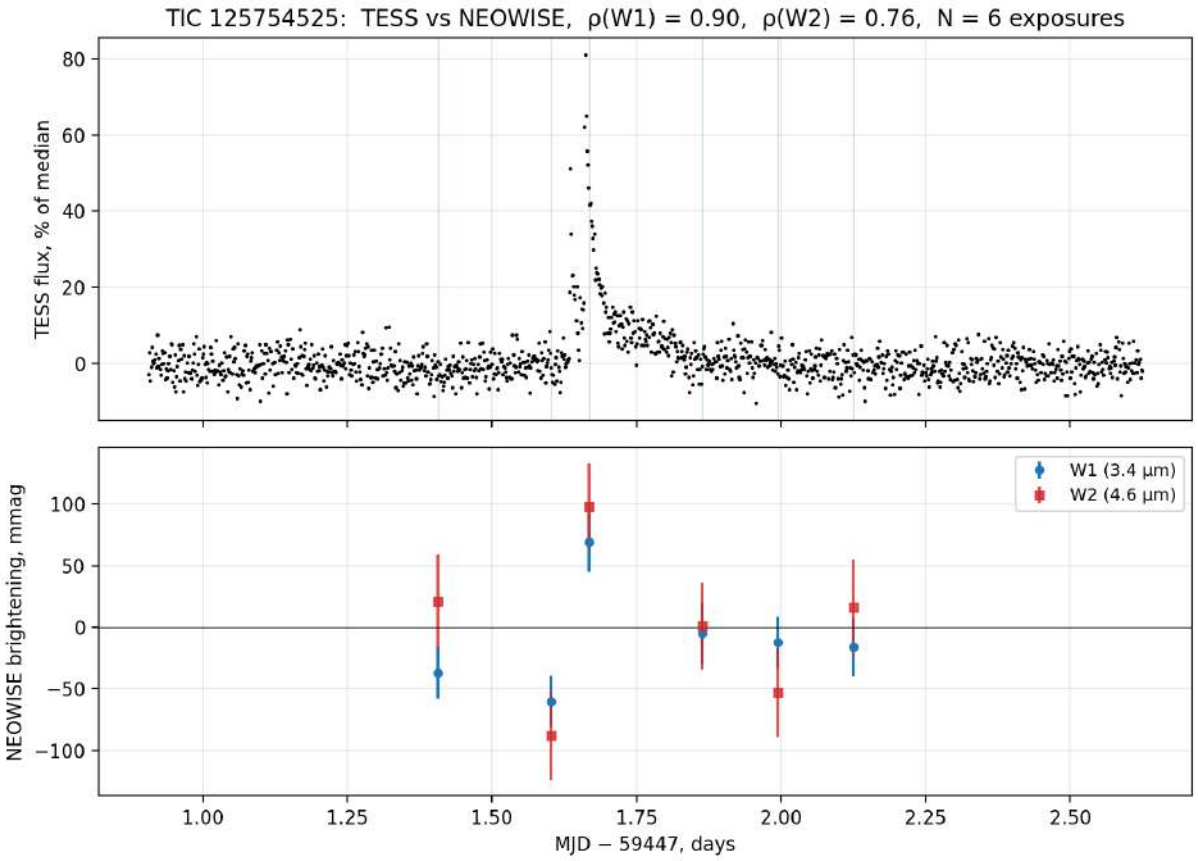

Figure 1: TIC 125754525 (Pleiades, catalogue of Seli et al. 2025, TESS Sector 42): the TESS light curve (top, in per cent of the series median; the vertical lines mark the WISE exposures) and the NEOWISE brightening in W1 and W2 relative to the quiescent level in these exposures (bottom), with the catalogue errors; ρ in the title is the correlation of the TESS flux at the exposure times with the infrared brightening and N the number of exposures. The WISE exposure 9 min after the peak of a flare with an amplitude of 80%, when the TESS flux was 45% above the quiescent level, shows a brightening of 70 ± 25 mmag in W1 and 100 ± 35 mmag in W2 (about 3σ in each band). The full combined figures are shown in Appendix A.

than the search interval); the scatter is the robust estimate 1.4826 MAD, where MAD is the median absolute deviation, but not smaller than the median error of a single exposure. The median and the MAD, unlike the mean and the variance, are insensitive to individual outliers, of which single-exposure photometry contains many. At least 15 such exposures are required — with fewer, the relative error of the scatter exceeds 30%, and the star is excluded from the statistics. The deviation of an exposure, Δ = (level − measurement), is positive for a brightening and is also expressed in units of the scatter (z); for a mean over n exposures, the scatter is divided by $\sqrt{n}$. The level is taken over all series of the mission. In doing so, one has to allow for a slow, brightness-dependent drift of the NEOWISE single-exposure photometry (known from the data releases; Cutri et al., 2015): for the stars of the Seli et al. (2025) sample, it amounts to about 20 mmag in W2 and 5 mmag in W1 between 2014 and 2024, mostly as a step in 2017–2019 (Appendix B). For the search for individual events and for the figures, the drift is immaterial (it shifts z by at most 0.5); for the averaging over hundreds of flares (Section 5), it is removed by comparing the flare windows with control windows in the same observing series. Stars brighter than the onset of saturation of the single exposures (W1 ≈ 8.0, W2 ≈ 7.0 mag; Cutri et al. 2015) are excluded from the averaging, not from the search for individual events. The formal definitions of all quantities are collected in Appendix B.

Time intervals. For every flare, two sets of exposures are considered. The averaging window of half-width 0.2 d (up to six consecutive exposures of one series, typically two to four clean ones) gives the mean deviation of the flare and its significance; these serve for averaging the deviations over all flares (stacking) and for the upper limits (Section 5). The search interval from −0.75 to +2.0 d serves for the search for individual events: within it, the extreme deviations on either side of the peak and the times of the nearest exposures before and after the peak are recorded, and an exposure falling between the catalogued start

doi: https://doi.org/10.52526/25792776-26.73.2-227

and end of the flare is marked as taken during the flare. The asymmetry of the interval reflects the fact that a response follows the flare and may last from hours to a day (Section 6); the part before the peak is retained to monitor the state of the star before the flare and to reveal events of the opposite sign. A flare is considered to be "in the search interval" if at least one clean exposure falls in it. For a star with several flares in one series, the windows of different flares may overlap; each exposure is then attributed to the flare nearest in time.

Thresholds. Deviations with $|z| \geq 2.5$ are marked in the figures; an event is treated as a candidate and verified frame by frame when $|z| \geq 4$ in one band, and in the reverse search (Section 7) in both bands. The shape criterion — a ratio of decay to rise duration $r \geq 1.5$ with a rise no longer than 60 min — corresponds to the classical flare profile (Davenport et al., 2014), whereas an eclipse egress or a pulsation gives a nearly symmetric profile; the criterion is not applied to events without a known peak time. All the parameters listed are input quantities of the program and may be changed in a repeated run; the adopted values follow from the considerations above but remain conventional, and this should be kept in mind when interpreting the numbers of events "in the interval", the limits, and the candidate list.

The limitations of the method follow from the data themselves. A WISE exposure lasts 7.7 s and is repeated after 95 min, whereas a typical TESS flare lasts minutes (median half-decay time 7 min according to Seli et al. 2025): the probability that an exposure falls on the flare itself is small, and the search is aimed primarily at the afterglow and at reprocessing lasting from hours to a day. For Kepler and K2 the 30-min cadence gives the peak time to within ±15 min and underestimates the amplitudes: the flux at the instant of a 7.7-s WISE exposure can exceed the cadence-averaged maximum several times, which is the main uncertainty when the optical and infrared amplitudes of an individual flare are compared. Finally, stars brighter than W1 ≈ 8 mag are saturated, and in crowded fields (the Pleiades, low Galactic latitudes) the 6″ WISE point-spread function does not resolve neighbouring stars.

3.3 Identification and proper motion

The catalogue coordinates refer to epoch 2000.0, whereas the NEOWISE observations were made in 2014–2024. In a cone search of 3″ radius around a fixed position, a star with proper motion μ leaves the circle by the year $2000 + 3''/\mu$: for $\mu > 0.12''$ yr^{-1} the late exposures are lost, and for $\mu > 0.2''$ yr^{-1} almost all of them. In the sample of nearby M dwarfs, such stars are numerous: 2757 of the 13 544 stars of the Seli et al. (2025) catalogue have $\mu > 0.12''$ yr^{-1}, and these are precisely the nearest, i.e., the infrared-brightest, stars. A check against the TIC proper motions showed that at $\mu > 0.2''$ yr^{-1} 45–64% of the stars had no measurement at all, while among those found at $\mu = 0.12$–$0.3''$ yr^{-1} the series ended before 2023 for 67–78% (median number of epochs 172 instead of ∼300).

For such stars, the search is made in a circle around the position propagated to the mid-survey epoch (2019.0), with a radius of $3'' + 5.5\,\mathrm{yr}\cdot\mu + 1''$ but not larger than 15″, after which only measurements within 3″ of the expected position of the star at the time of each frame are kept. The identification precision remains the same, but the motion of the star is now taken into account, and stationary neighbours are rejected. For the Seli et al. (2025) catalogue this recovered measurements for 694 of the 918 stars that had no epochs at all (median $\mu = 0.30''$ yr^{-1}) and completed the truncated series of 1583 stars (median number of epochs 85 → 324, last epoch 2019 → 2024). After the correction, the completeness of the series no longer depends on μ: in all intervals, the median is 300–360 epochs and the fraction of truncated series is 0–2%. For cluster members (the Feinstein et al. 2024 and K2 catalogues) no correction is needed: their displacement over 20 years is below 1″.

3.4 Program output

The program produces text tables — NEOWISE measurements, quiescent levels, simultaneity, deviations per flare, infrared and optical amplitudes per observing series, star classes — and the cleaned flare catalogue; the summary of Section 4 is built from the simultaneity table, and the material of Section 7 from the amplitude table. The volume of the processing: the NEOWISE measurement table (Section 2.2) occupies about 600 MB, the simultaneity table contains 226 000 rows, and about 1700 combined figures for 1180 stars have been produced and inspected. A combined figure is drawn for every WISE observing series that contains at least one flare with an exposure in the search interval; its panels and notation are described in Appendix A, and examples are given in Figs. 1 and A1–A4. A detailed description of the input parameters and output tables will be given in a separate paper on the program.

4 Geometry of simultaneous observations of flares and infrared emission

A ten-year overlap of two surveys in time does not by itself imply simultaneous observations of the same stars. TESS observes each sector for 27 d in the anti-solar direction (elongation about 180°), whereas WISE scans a great circle at a solar elongation of about 90° (in practice, 82–98°, as the scan is shifted ahead of or behind the quadrature). These regions intersect only near the ecliptic poles, through which the WISE circle passes on every orbit, and which TESS Camera 4 reaches in every sector of its hemisphere. The exception is Sectors 42–46 (2021–2022), when TESS was pointed along the ecliptic: during the 27 d of a sector, the Sun moves by 27°, and the WISE circle passes across the edge of the field. In this way, during the first days of Sector 42 (2021 August 20–25) the Pleiades, lying at the edge of the Camera 4 field, entered the WISE scanning strip; in Sector 43 the WISE circle passed east of them, across Camera 4 at $\lambda \approx 85$–$97°$, where about thirty more field stars from the Seli et al. (2025) and Feinstein et al. (2024) catalogues received simultaneous exposures. The field of the Kepler space telescope is fixed and lies at $|\beta| \approx 65°$, so that WISE crossed it twice a year (April–May and October–November 2010 in the AllWISE data). The K2 fields, on the contrary, lie on the ecliptic, and during the 80 d of a campaign, the WISE circle crosses each of them exactly once: K2 is therefore the most suitable partner of NEOWISE for such comparisons.

This geometry is shown in Fig. 2: in the ecliptic plane (a) the TESS field and the WISE scanning plane never intersect, while on the sky (b) their overlap region is a circle of about 12° radius around the ecliptic pole, covered by Camera 4; at $15° < |\beta| < 75°$ there is no overlap, which explains the zeros in Table 2 for intermediate latitudes, and the Kepler field at $\beta \approx 65°$ lies outside this region. Panel (c), based on the actual pointings of Sectors 42 and 43, shows how the meridian of the WISE circle crossed Camera 4 over the Pleiades during the first day of Sector 42.

The summary for the five catalogues (Table 2, Fig. 3) confirms this picture quantitatively. In the three TESS catalogues there is not a single flare with a WISE exposure in the search interval at $15° < |\beta| < 75°$ — among nine thousand stars and about a hundred thousand flares; at $|\beta| > 75°$ such flares exist for 38–73% of the stars, and at $|\beta| < 15°$ for 5–7% of the stars of the Feinstein et al. (2024), Seli et al. (2025) and K2 samples (Sectors 42–43 for TESS, Campaign 4 for K2; none in the Yudovich et al. (2025) sample). Overall, the fraction of flares in the search interval is 1–3% for TESS, 0.8% for Kepler (two short observing series over the four years of the mission), and 2.4% for K2, and about 1700 flares from all catalogues together lie within six hours of the peak, 740 of them within one hour.

Table 2: Simultaneity of flares and WISE exposures. “In the search interval”: at least one clean exposure between −0.75 and +2 d of the peak.

Catalogue	Flares / stars	In the search interval: flares / stars	Exposure within 1 h / 6 h	Median time to nearest exposure, d
Feinstein et al. (2024) (TESS)	11 744 / 1887	156 / 91	35 / 97	60
Yudovich et al. (2025) (TESS)	9 754 / 225	264 / 48	58 / 164	56
Seli et al. (2025) (TESS)	122 958 / 12 245	1936 / 707	471 / 1178	61
Yang & Liu (2019) (Kepler × AllWISE)[a]	79 287 / 1742	599 / 403	165 / 280	269
Ilin et al. (2021) (K2)[b]	2 544 / 841	60 / 56	13 / 26	36

[a] Two AllWISE observing series in 2010.
[b] Pleiades, Campaign 4: 55 flares / 51 stars; Hyades, Campaign 4: 5 / 5; Praesepe, Campaign 5: none.

For K2 both outcomes are instructive. The WISE observing series of the Pleiades and Hyades fell within the first eight days of Campaign 4 (February 2015): 55 flares of 51 Pleiades stars received an exposure in the search interval, 13 of them within an hour, with thirty clean exposures per star per series. The observing series of Praesepe ended on 2015 April 26, one day before the start of Campaign 5, and simultaneous observations there are absent. Together with TESS Sector 42, the Pleiades turn out to be the only cluster with two epochs of simultaneous optical and mid-infrared flare observations — 2015 and 2021, about a hundred flares of ninety coeval stars.

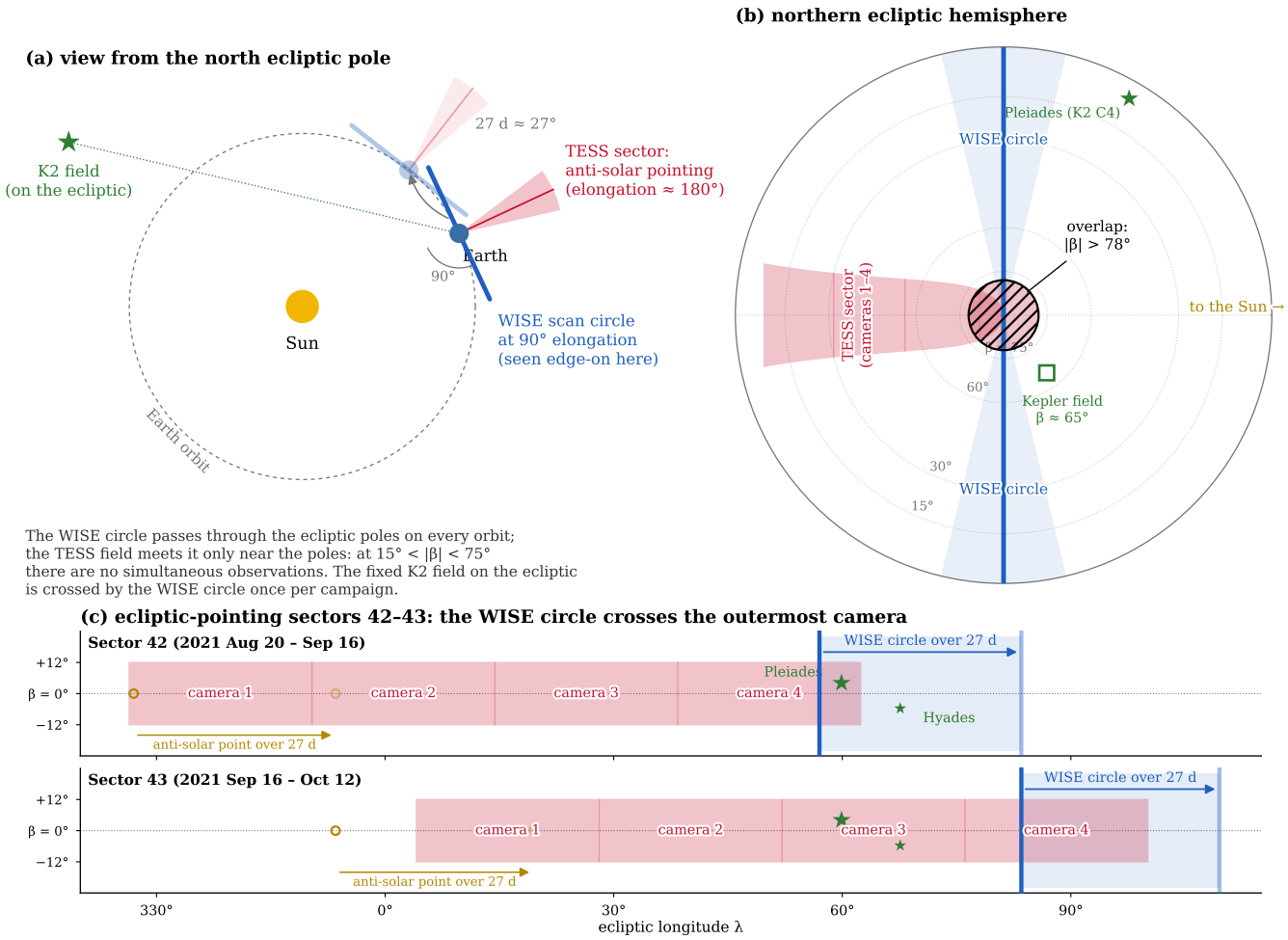

Figure 2: Geometry of simultaneous TESS and WISE observations. (a) View from the north ecliptic pole: the Sun, the Earth's orbit and the Earth at two moments 27 d apart; the red sector is the TESS field in the anti-solar direction, the blue line is the WISE scan circle at ≈ 90° elongation seen edge-on, the green star is the fixed K2 field on the ecliptic. (b) The northern ecliptic hemisphere in polar projection (radius = $90° - \beta$): the TESS sector (Cameras 1–4), the WISE circle with the band of its displacement over 27 d, the hatched overlap region at $|\beta| \gtrsim 78°$, the Kepler field ($\beta \approx 65°$) and the Pleiades ($\beta \approx 4°$). (c) Sectors 42 and 43 with ecliptic pointing, from the actual camera centres: rectangles are Cameras 1–4, the blue line and band are the meridian of the WISE circle at the start of the sector and its displacement over 27 d, the yellow circles are the anti-solar point at the start and end of the sector, the green stars are the Pleiades and the Hyades.

5 Preliminary upper limits

The averaging is performed over the flares of the cleaned catalogs that pass the quality selection of Section 2 (at least five points and an amplitude of at least five times the scatter), have at least one clean exposure in the ±0.2 d window, and at least one quiescent exposure in the same observing series. Each flare enters with unit weight, and the flare-averaged response $\hat{D}$ is the trimmed mean of the window means (10% discarded at either end, as protection against isolated frame defects). Its reference value in the absence of a response, μ_0, is not zero because of the drift described in Section 3.2 and is obtained from control windows placed at random quiescent epochs of the same star in the same observing series; the uncertainty s of the difference $\hat{D} - \mu_0$ is obtained by a bootstrap over stars, since the flares of one star are not independent. The one-sided 95% upper limit on a brightening is $U_{95} = \max(\hat{D} - \mu_0, 0) + 1.645\, s$; when the deviation is negative, the limit equals $1.645\, s$ and is set by the noise alone. For the colour W2−W1 a positive deviation is a reddening. The construction is described in Appendix C.

For the Seli et al. (2025) catalogue, 796 flares of 376 stars satisfy these conditions (2.6 clean exposures per window on average; the median scatter of the quiescent level is 17 mmag in W1 and 20 mmag in W2).

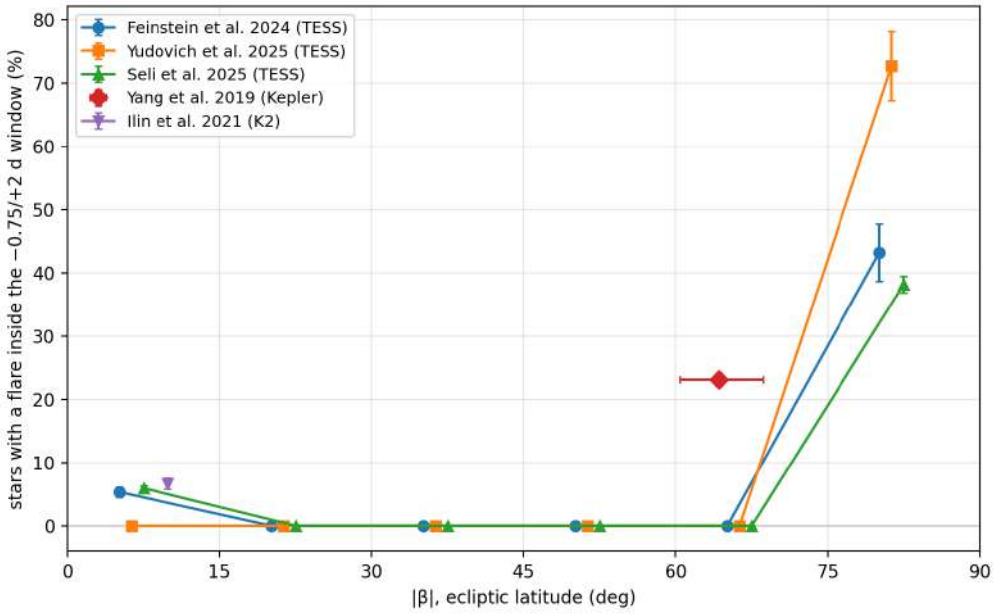

Figure 3: Fraction of stars with at least one flare having a clean WISE exposure in the search interval from −0.75 to +2 d of the peak, as a function of the absolute ecliptic latitude, for the five catalogues. The Kepler field is shown by a single point with the spread of latitudes across the field. Between 15° and 75° there are no simultaneous TESS and WISE observations.

Because of the observing geometry (Section 4), all but nine of them belong to stars at $|\beta| > 75°$: near the ecliptic, the series lasts about a day and has no quiescent exposures outside the exclusion zones of the flares. The flare-averaged deviation is consistent with zero in all three quantities: $\hat{D} - \mu_0 = 0.0 \pm 0.6$ mmag in W1, -0.8 ± 0.7 mmag in W2 and -0.9 ± 0.7 mmag in W2−W1; the W2 and colour deviations are one and the same quantity, the W1 deviation being zero, and they vanish when the control windows are restricted to ±3 d of the flare. The upper limits on a brightening are $U_{95} = 0.96$ mmag in W1, 1.13 mmag in W2 and 1.23 mmag in W2−W1, all set by the noise (Fig. 4). For Kepler, 129 flares of 118 stars have a clean AllWISE exposure in the window and a quiescent exposure in the same series (3.7 exposures per window; the AllWISE single-exposure photometry is twice as noisy, 31 mmag in W1 and 46 mmag in W2). The two AllWISE series of the Kepler field, April–May and October–November 2010, belong to the cryogenic and the post-cryogenic phases of the mission and are offset by +10 mmag in W1 and +31 mmag in W2 (median over the field, the stars being fainter in the second series; the offset grows towards fainter stars), so that here too the comparison within the series is essential. The deviations are -1.5 ± 3.0 mmag in W1 and -5.4 ± 3.9 mmag in W2, consistent with zero, and $U_{95} = 4.9$ and 6.4 mmag. The division of the samples by stellar temperature and flare amplitude is deferred to the recalculation announced below.

What do these limits mean physically? The limit of 0.96 mmag states that, averaged over ±0.2 d around the flares of the sample, the excess at 3.4 μm does not exceed 0.09% of the stellar flux. A flare of the sample, however, occupies a very small part of this window: the median equivalent duration of the 796 flares is 33 s (16th–84th percentiles 11–111 s), so that even the optical flare flux itself, averaged over the 0.4 d window, amounts to $\sim 10^{-3}$ of the stellar flux, and the infrared emission of the flare (Section 6) and its reprocessing by hot dust, which lasts as long as the flare, are diluted by the same factor. The window-averaged limit therefore does not yet constrain either of them; it is a methodological result, which demonstrates the absence of systematic effects at the level of about 1 mmag and bounds only a response lasting a substantial part of the window, i.e. hours (a long-lived afterglow or a post-flare dimming). Physical constraints on the flare emission and on dust reprocessing require exposures within minutes of the peak, such as the K2 events of the Pleiades (Section 7), or a window matched to the flare duration. A recalculation of the limits on all five samples, with a window matched to the flare duration, split by flare amplitude and stellar temperature, will be the subject of a separate paper.

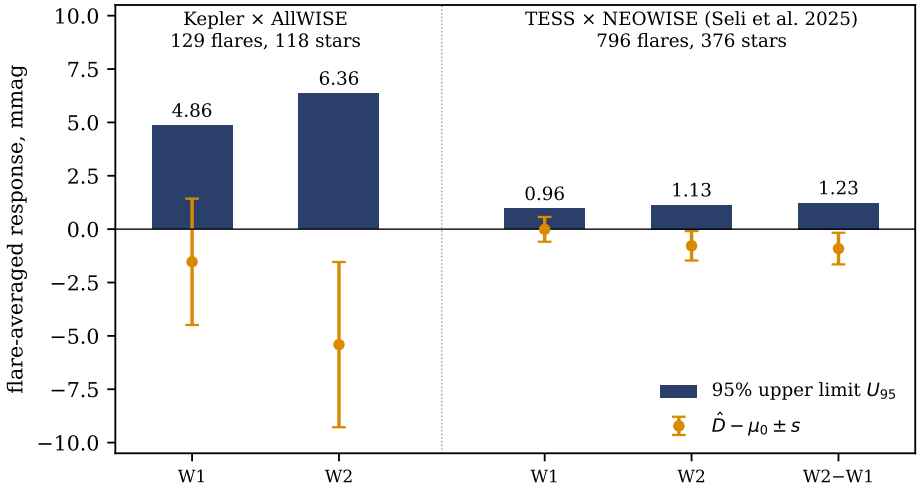

Figure 4: 95% upper limits on the flare-averaged infrared brightening within ±0.2 d of the peak, Eq. (C2), on the cleaned catalogues, with control windows in the same observing series as the flare: Kepler × AllWISE (129 flares of 118 stars; W1 and W2) and TESS × NEOWISE (796 flares of 376 stars of the Seli et al. 2025 catalogue; W1, W2 and the colour W2−W1, for which a positive deviation is a reddening). The points with error bars show the flare-averaged deviation relative to the null, $\hat{D} - \mu_0$, with the uncertainty s from the bootstrap over stars.

6 Expected infrared manifestations of a flare and their magnitude

Before turning to individual events, we estimate what changes of the infrared brightness, and with what delay, may accompany an optical flare. The estimates are made for a flare with an amplitude of 10% in the TESS band and a duration of 10 min on an M dwarf with a photospheric temperature of 3300 K; at the peak of such a flare its luminosity is about 0.1 $L_{\rm bol}$ of the star (Osten & Wolk, 2015).

The flare's own emission. The optical continuum of a flare is close to black-body emission with a temperature of $\sim 10^4$ K (Hawley & Fisher, 1992; Kowalski et al., 2013). At 3.4 and 4.6 μm the emission of both the photosphere and the flare follows the Rayleigh–Jeans law, and the ratio of their surface brightnesses equals the ratio of the temperatures, whereas in the TESS band it is many times larger. For a flare occupying a fraction x of the visible disc and radiating as a black body of temperature $T_{\rm f}$ above a photosphere of temperature T_*, the relative amplitude in a band with response $S_b(\lambda)$ of a photon-counting detector is

$$A_b = x\,\frac{\int B_\lambda(T_{\rm f})\,S_b(\lambda)\,\lambda\,d\lambda}{\int B_\lambda(T_*)\,S_b(\lambda)\,\lambda\,d\lambda}, \qquad (1)$$

where A_b is the relative flare amplitude in band b, x the fraction of the visible disc covered by the flare, B_λ the Planck function, $T_{\rm f}$ and T_* the temperatures of the flare and of the photosphere, and $S_b(\lambda)$ the response of the band (the factor λ accounting for photon counting); the ratio $A_{\rm opt}/A_{W1}$ does not depend on x; in the Rayleigh–Jeans range the integrand ratio reduces to $T_{\rm f}/T_*$. A brightening of Δ mmag corresponds to a flux excess $A = 10^{0.4\Delta/1000} - 1$. Consequently the flare amplitude in the W1 and W2 bands is about ten times smaller than in the TESS band (9–15 times for photospheric temperatures of 3000–3500 K and flare temperatures of 8000–12 000 K): a flare with an amplitude of 10% in the TESS band produces a brightening of about 10 mmag in W1 and 9 mmag in W2, with a slight decrease of the colour index W2−W1, simultaneously with the flare and of the same duration. Averaged over the ±0.2 d interval, such an event leaves ≈ 0.2 mmag, and over the catalogue, where the median flare amplitude is about 1%, hundredths of a milli-magnitude: the flare-averaged response of the flares' own emission is well below our limits, a null result of the averaging over flares is expected in this case, and this response can be measured only from individual exposures taken within minutes of a strong flare (Fig. 1: a brightening of 70 mmag in W1 at a moment when the TESS flux was 45% above the quiescent level, i.e. an amplitude ratio of ≈ 7, consistent within the errors with the expected 9–15). This is compatible with the limits of 5–8 mmag on the continuum in J, H and K_s (Section 1). The estimate is made for a black body; according to radiative-hydrodynamic models with deep atmospheric heating (Kowalski et al., 2024; Mamonova et al., 2025) the infrared amplitude may differ, and

doi: https://doi.org/10.52526/25792776-26.73.2-227

its calculation over the model grid is a separate task.

Reprocessing by circumstellar dust. Dust that intercepts a fraction f_d of the stellar radiation ($f_d \approx L_{\rm IR}/L_*$) intercepts the same fraction of the flare energy and re-emits it thermally. The W1 and W2 bands are sensitive to the emission of dust with temperatures of 500–1500 K; around an M dwarf such dust is located 0.005–0.05 au from the star, which the flare light reaches in seconds, so that this response too is simultaneous with the flare and lasts as long as the flare; it is stronger in W2 and is accompanied by a reddening of the colour. Its amplitude is approximately $0.5\,f_d$ of the stellar flux: about 50 mmag for $f_d \approx 0.1$ (young stars with residual discs; Williams & Cieza 2011), 0.5 mmag for $f_d \approx 10^{-3}$ (the brightest debris discs; Wyatt 2008) and below 0.05 mmag for $f_d < 10^{-4}$, typical of field M dwarfs. A delay of a day is impossible for a dust "echo": matter at a distance of a light-day (∼170 au) has a temperature of ∼10 K and does not radiate in W1 or W2. A dust response of this kind can be detected only in exposures taken during the flare itself: its amplitude follows the flare, $\approx 5 f_d\, F_{\rm fl}(t)/F_*$, where $F_{\rm fl}(t)$ is the flare flux in the optical band at time t, F_* the quiescent flux of the star in the same band, and the factor 5 corresponds to the amplitude $0.5 f_d$ of the reference flare with $F_{\rm fl}/F_* = 0.1$; averaged over a window of duration T the amplitude is $\approx 5 f_d\,{\rm ED}/T$, where ${\rm ED} = \int F_{\rm fl}(t)\,{\rm d}t/F_*$ is the equivalent duration of the flare, i.e. $\approx 5\times10^{-3} f_d$ for the flares of Section 5, so that the present limit corresponds only to $f_d \lesssim 0.2$. It should be sought in individual events, above all among the members of the young groups of the Feinstein et al. (2024) catalogue.

Dimming and pre-peak changes. An infrared dimming may arise from the increased opacity of the H^- ion in the chromosphere heated by the flare — this is how the "negative flares" and brightness dips known in the optical since the 1970s were explained (Aboudarham & Henoux, 1987; Doyle et al., 1988; Giampapa et al., 1982; Henoux et al., 1990; Leitzinger et al., 2014; Rodonò et al., 1979; Tovmassian et al., 2003; Ventura et al., 1995) — or from an ejection of matter, by analogy with the coronal dimmings on the Sun and on stars (Veronig et al., 2021); no expected amplitudes at 3–5 μm are available in the literature, and our estimates of the flare-averaged response (consistent with zero) and the upper limits on a brightening are the first such estimate. The part of the search interval before the peak is retained because brightness dips are observed within half an hour before the impulsive phase, with amplitudes of 1–20% and durations from seconds to tens of minutes (summary in Bruno et al., 2024), and in the model of Tovmassian et al. (2003) they are explained by a growth of the spot area before the flare, which should manifest itself in the infrared as well, in the same way as rotational modulation (Section 7); in addition, the peak listed in a catalogue may not be the first event in a group of flares, and the flare time may coincide with an eclipse or rotational phase at which the star deviates from its quiescent level in the infrared as well.

From these estimates follows the search strategy: the flare-averaged response over a window of hours constrains only a long-lived response (an afterglow or a post-flare dimming), while both the flare's own emission and its reprocessing by dust are to be sought in individual exposures within minutes of strong flares, the dust "echo" above all in young stars; the few W2 brightenings 0.3–1 d after a flare found during the inspection (e.g. the point at $\tau = +0.7$ d in Fig. A4) are not explained by any of these mechanisms and require, first of all, a verification of the frame quality and of the observing series.

7 By-products

The combined figures for hundreds of stars revealed phenomena that were not among the aims of the search but are necessary for its correct interpretation.

Infrared variability outside flares. At a 95-min cadence and with observing series 1–8 d long, NEOWISE traces eclipses and rotational modulation with periods from several hours to a week. An example is the eclipsing system TIC 382069435 (Fig. 5): over an eight-day observing series 37 WISE exposures reproduce both the eclipse, reaching 33% below the median, and the smooth wave of rotational modulation in the TESS light curve; the correlation of the TESS flux at the exposure times with the brightening in W1 is 0.98, and in W2 0.95. The ratio of the infrared and optical amplitudes depends, for eclipses, on the temperature ratio of the components and, for spots, on the spot contrast at 3–5 μm; a systematic period search over 10–20 observing series spanning the eleven years of the survey for all 13 500 stars of the Seli et al. (2025) catalogue is a separate task, which the program makes feasible.

Spurious catalogue flares. The same figure shows six catalogue "flares" falling exactly on the eclipse edges: the detection algorithm takes the rapid egress from an eclipse for the rise of a flare. In the averaging over flares such events would produce a spurious infrared "response" of either sign, because at these moments the star does indeed change its infrared brightness. The shape criterion (a decay no shorter than 1.5 times

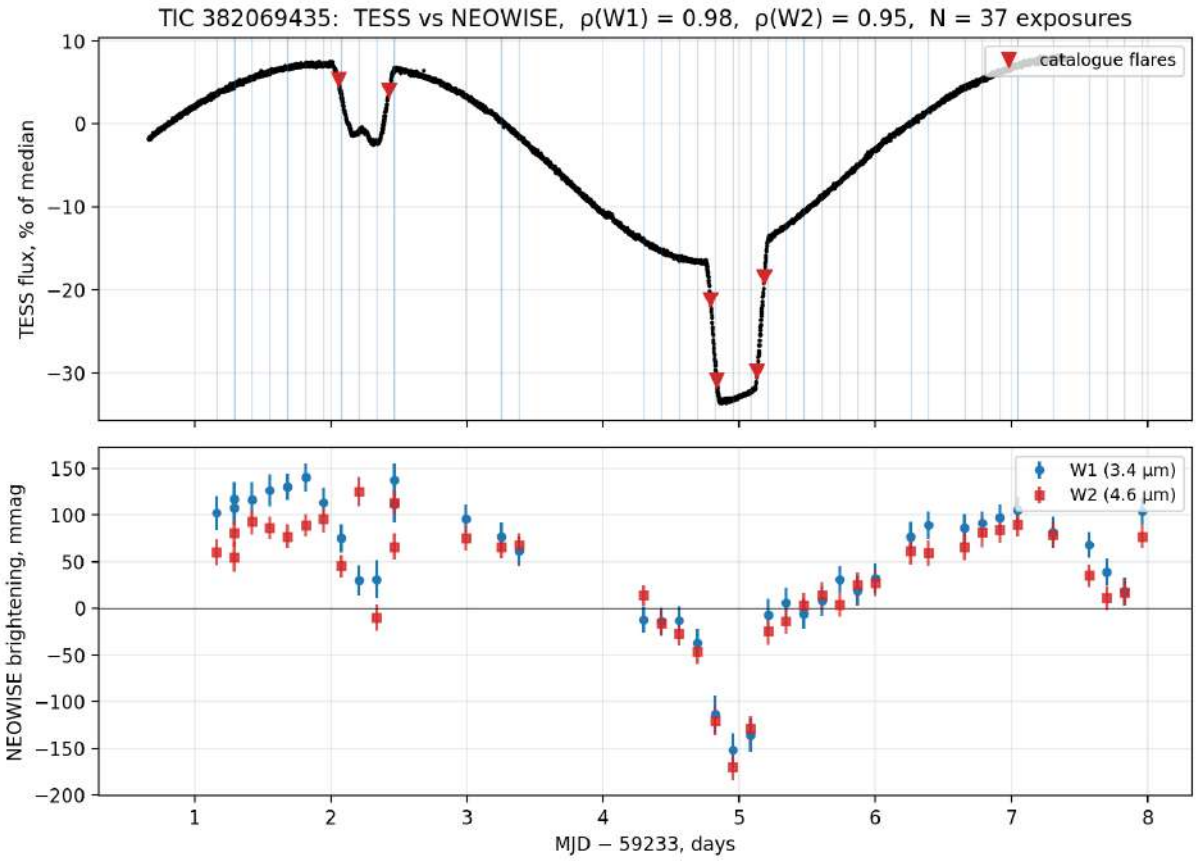

Figure 5: The eclipsing system TIC 382069435: the TESS light curve and 37 NEOWISE exposures of a single eight-day observing series; the correlation of the TESS flux at the exposure times with the brightening in W1 is 0.98, in W2 0.95. Triangles mark catalogue "flares" coinciding with the eclipse edges.

the rise) and the classification of eclipsing and pulsating stars remove them from the cleaned catalogue; the comparison with the infrared series thus serves as an independent means of checking flare catalogues.

Individual events within hours of a flare. For hundreds of flares a WISE exposure lies within an hour of the peak (Table 2). An example is TIC 125754525 in the Pleiades (Fig. 1): a flare with an amplitude of 80% in the TESS band, a WISE exposure nine minutes after the peak, on the decay, when the TESS flux was 45% above the quiescent level, and a brightening of 70 ± 25 mmag in W1 and 100 ± 35 mmag in W2. The ratio of the optical and W1 flare fluxes at that moment (≈ 7) is consistent, within the errors, with a hot continuum against the photosphere of an M dwarf (9–15). By itself such a case, below the formal threshold $|z| \geq 4$ but at the 3σ level in both bands simultaneously, and in an observing series of uneven frame quality, remains a candidate; it indicates where to search — in clusters with two epochs of simultaneous observations and in stars near the ecliptic poles — and it is there, among the K2 events in the Pleiades, that two flares with brightenings at 13.5σ and 6.3σ have been found, which are the subject of a separate article. For every candidate the program provides the quality indicators of all frames of the observing series, image cut-outs and a list of Gaia neighbours, which allows cosmic-ray hits, frame defects and blending with a neighbouring star to be excluded.

Reverse search. The quiescent level and the z value of every exposure also allow a reverse search: from an infrared anomaly ($|z| \geq 4$ in both bands) to the optical light curve at the same moment. In this way flares missed by the catalogues, and events with no optical counterpart at all, are found; for the K2 campaigns such a search is currently in progress.

8 Conclusions

A program for cross-matching optical flares with WISE single-exposure photometry has been built and tested on five catalogues. The main results are: (1) simultaneous TESS and WISE observations are determined by the pointing geometry and are concentrated near the ecliptic poles and in a few ecliptic sectors,

doi: https://doi.org/10.52526/25792776-26.73.2-227

whereas the K2 campaigns provide them regularly; (2) the identification of nearby stars in a multi-year survey requires the proper motions to be taken into account, otherwise the nearest and infrared-brightest stars are lost; (3) the flare-averaged infrared response within ±0.2 d of the peak is below about 1 mmag in W1, W2 and W2−W1 for the TESS sample and below 5 mmag in W1 for Kepler, the limits being set by the noise; because a flare occupies a tiny part of such a window, these limits bound only a response lasting hours and do not yet constrain the flare's own infrared emission or its reprocessing by hot dust; an averaging over the flares of a multi-year survey must allow for the brightness-dependent drift of the NEOWISE photometry, which otherwise imitates a mean dimming of several mmag; (4) the combination of the two surveys provides an independent check of flare catalogues and material for the infrared periodicity of thousands of stars.

The main direction of further work is not the averaged response but individual events with a WISE exposure within minutes of a flare, above all in the Pleiades with their two epochs of simultaneous observations, as well as the members of young groups in which reprocessing by dust is possible (Section 6). Among the K2 events in the Pleiades (Section 7), two flares with simultaneous brightening in W1 and W2 at the flare peak, at 13.5σ and 6.3σ in W1, have been found; their analysis will be presented in a separate article.

Acknowledgements

This work makes use of data from the TESS, Kepler and K2 missions (NASA) and the MAST archive, of the WISE and NEOWISE surveys (NASA/JPL-Caltech, UCLA) and the IRSA archive, and of data from the Gaia mission (ESA) via the TIC and VizieR. The software used includes numpy, pandas, astropy (Astropy Collaboration et al., 2022), astroquery (Ginsburg et al., 2019) and lightkurve (Lightkurve Collaboration et al., 2018).

Appendices

Appendix A Examples of combined figures

The main results of the program are illustrated by the combined figures (Figs. 1 and A1–A4). They are drawn for every WISE observing series that contains at least one flare with an exposure in the search interval and consist of four or five panels with a common time axis (MJD). The top panel shows the optical light curve (TESS, Kepler or K2) in per cent of the median of the series; dashed vertical lines mark the catalogue flare peaks, and above each are the rise (↑) and decay (↓) durations in minutes and their ratio r; the label frame is green if the event passed the shape criterion, red if it did not, and grey if the peak time is unknown. The three middle panels show the deviations from the quiescent level in milli-magnitudes. The axis labels of the program, $-\Delta$W1 and $-\Delta$W2, refer to the deviation (measurement − level), so that the quantity plotted is the brightening Δ_{vj} of Eq. (B4) (positive upward means brightening); the colour panel shows the change of the colour index, $(\mathrm{W2}-\mathrm{W1})_{\mathrm{measured}}-(\mathrm{W2}-\mathrm{W1})_{\mathrm{level}}$, which is positive when the star becomes bluer (a relative brightening in W1), i.e. opposite in sign to the colour deviation of Section 5; the error bars are the catalogue errors of the individual exposures. The pink band around each flare is the ±0.2 d averaging interval (where the bands of neighbouring flares overlap, the colour is more saturated); the search interval from −0.75 to +2.0 d is not drawn as a band — the point-deviation labels refer to it. The labels in blue frames, "z = … (window, n = …)", give in these figures the z of the mean over ±0.75 d of the peak (the symmetric part of the search interval) and the number of exposures in it, not over the ±0.2 d averaging window of Section 5, which is marked by the pink band; the green labels, "z = … (point, τ = …)", give the largest point deviation in the search interval and its delay with respect to the peak, and this exposure is marked by a dash-dotted vertical line. The bottom panel is drawn only when $\max|z| \geq 4$ in W1and shows $-\Delta$W1 as a function of the time from the peak, τ, for all flares of the series aligned at the flare peak; the horizontal lines at ±2.5σ (i.e. $|z| = 2.5$) are the marking threshold, and the inset gives the quiescent-level scatter σ(W1), the median exposure error and the largest $|z|$. One figure shows one observing series; for stars with many series the figures are numbered in the order of the series. Four such figures are reproduced below as produced by the program; they were chosen to show the main types of what is encountered during the inspection: a response candidate with several exposures, a single deviation requiring frame-by-frame verification, an eclipsing system with spurious catalogue flares, and an example from the Kepler × AllWISE data in which the offset between the two AllWISE series imitates a response.

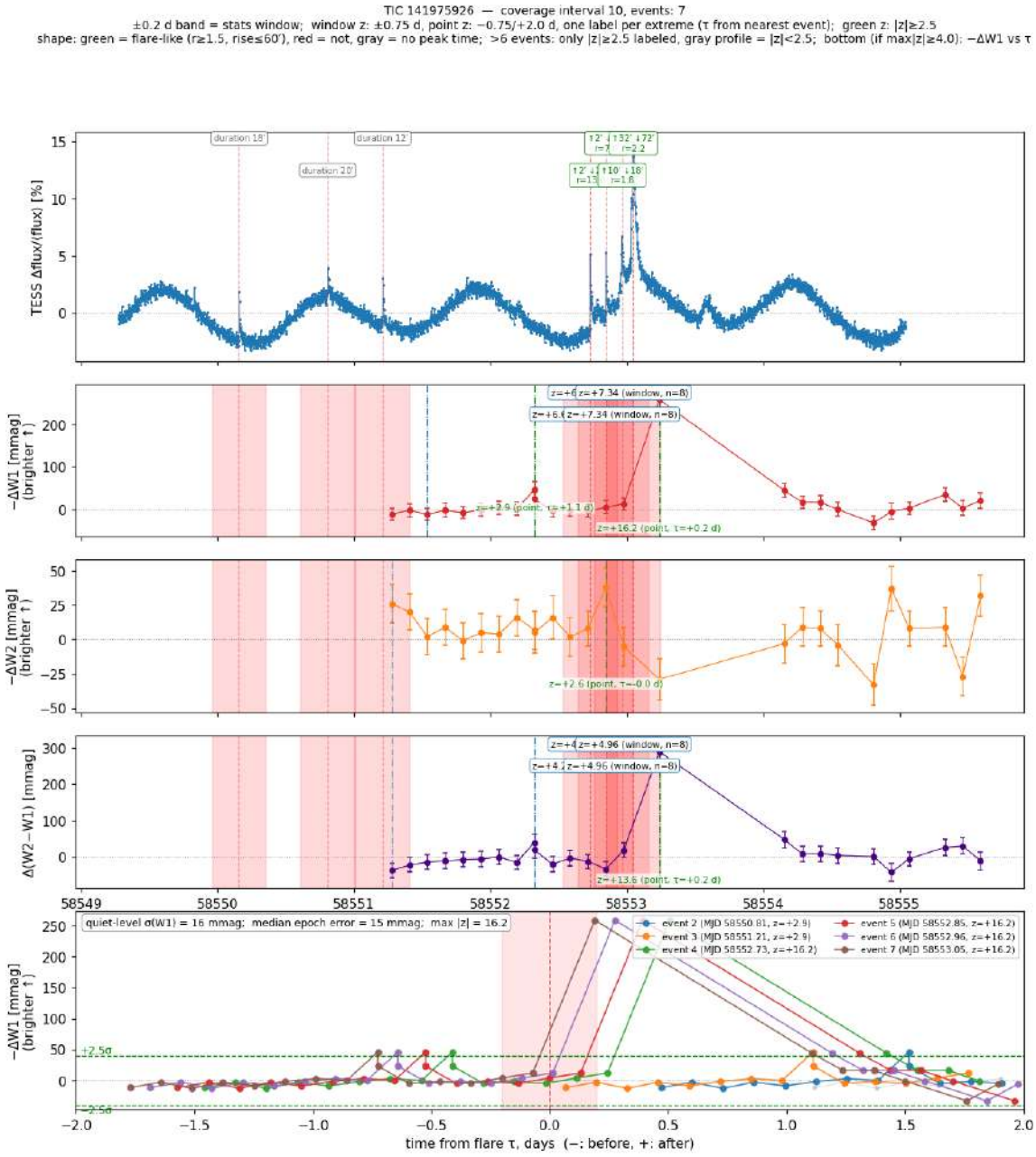

Figure A1: TIC 141975926 (catalogue of Seli et al. 2025), observing series 10: a group of four flares with amplitudes up to 14% superposed on rotational modulation. The mean W1 deviation over the eight exposures within ±0.75 d is $z = +7.3$, the point deviation $z = +16$ (≈ 250 mmag) at $\tau = +0.2$ d, in W2 only $z \approx +2.6$, the colour becomes bluer. A candidate requiring verification of the individual frames and of the neighbours.

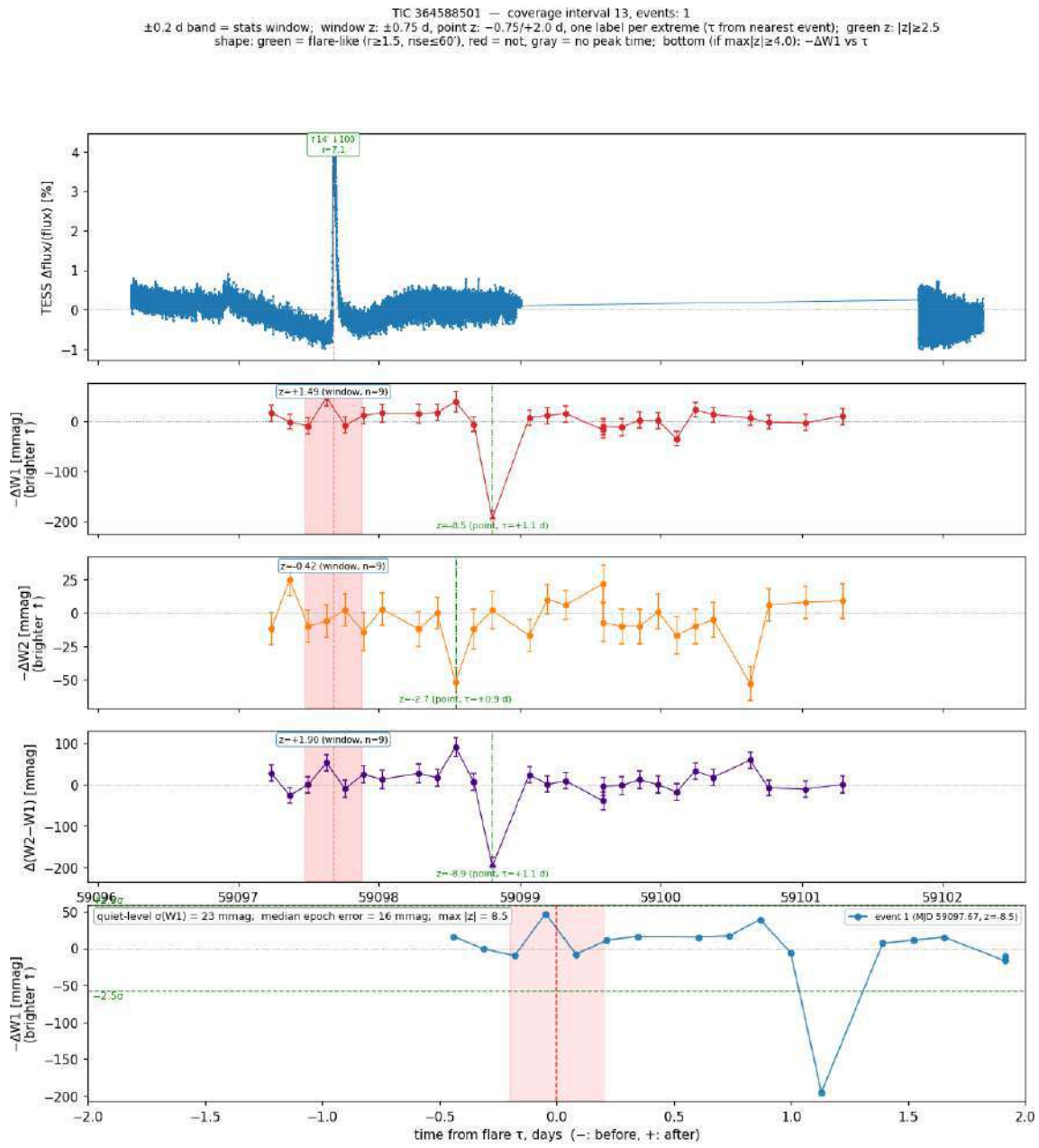

Figure A2: TIC 364588501 (catalogue of Yudovich et al. 2025), series 13: a single flare with an amplitude of 4% ($r = 7.1$). There is no deviation in the averaging interval, but one exposure at $\tau = +1.1$ d gives a dimming of 190 mmag in W1 ($z = -8.5$) while the W2 value in the same exposure is unremarkable (a weak W2 dip, $z = -2.7$, falls at $\tau = +0.9$ d). A typical single deviation: a candidate pending verification of the frame quality.

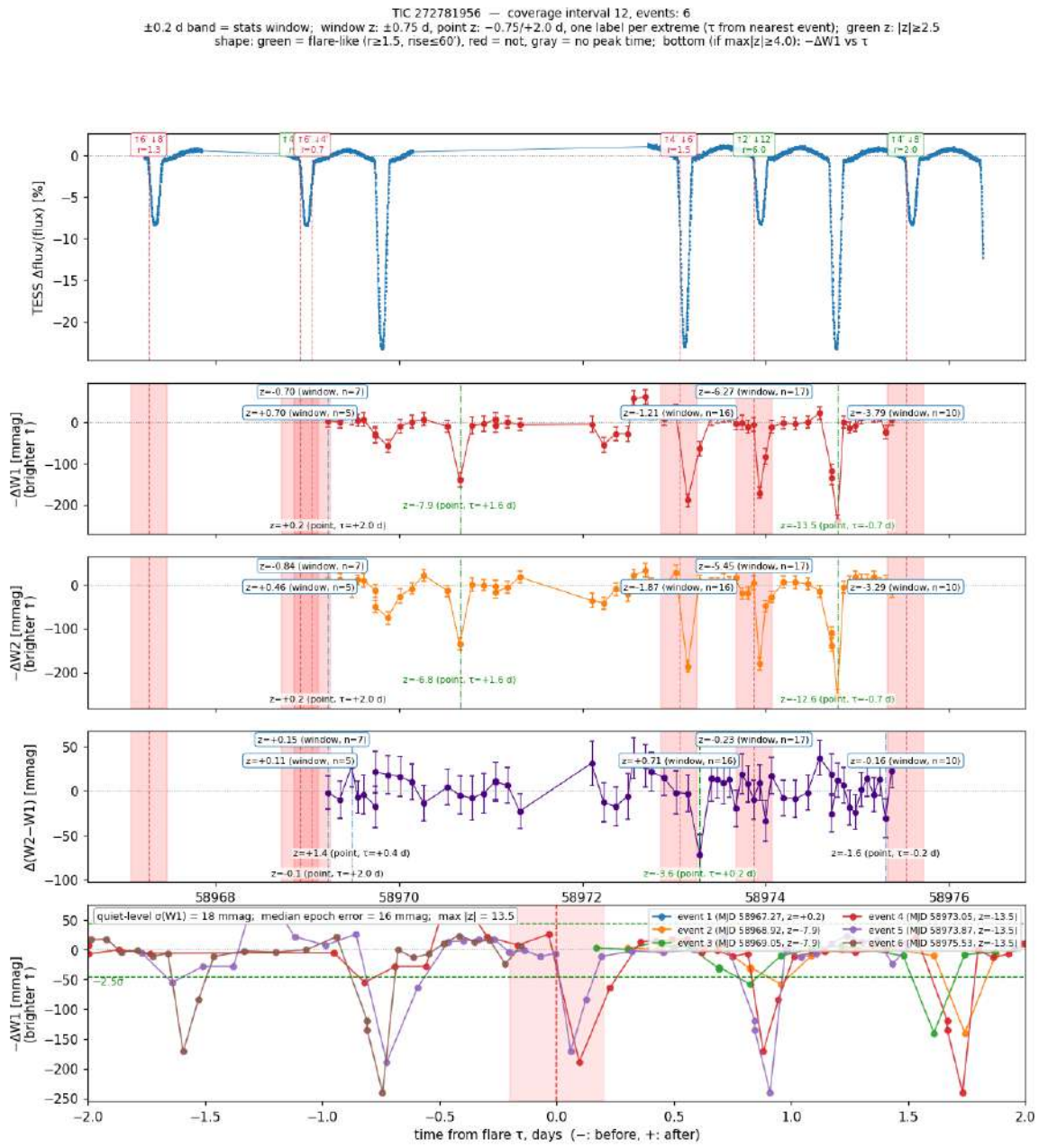

Figure A3: TIC 272781956 (catalogue of Seli et al. 2025), series 12: an eclipsing system with eclipses 8% and 23% deep; all six catalogue "flares" fall on eclipse egresses, and the shape criterion rejects three of them. The infrared curves reproduce the eclipses with synchronous dips in W1 and W2 at constant colour; the star is excluded by its classification as eclipsing.

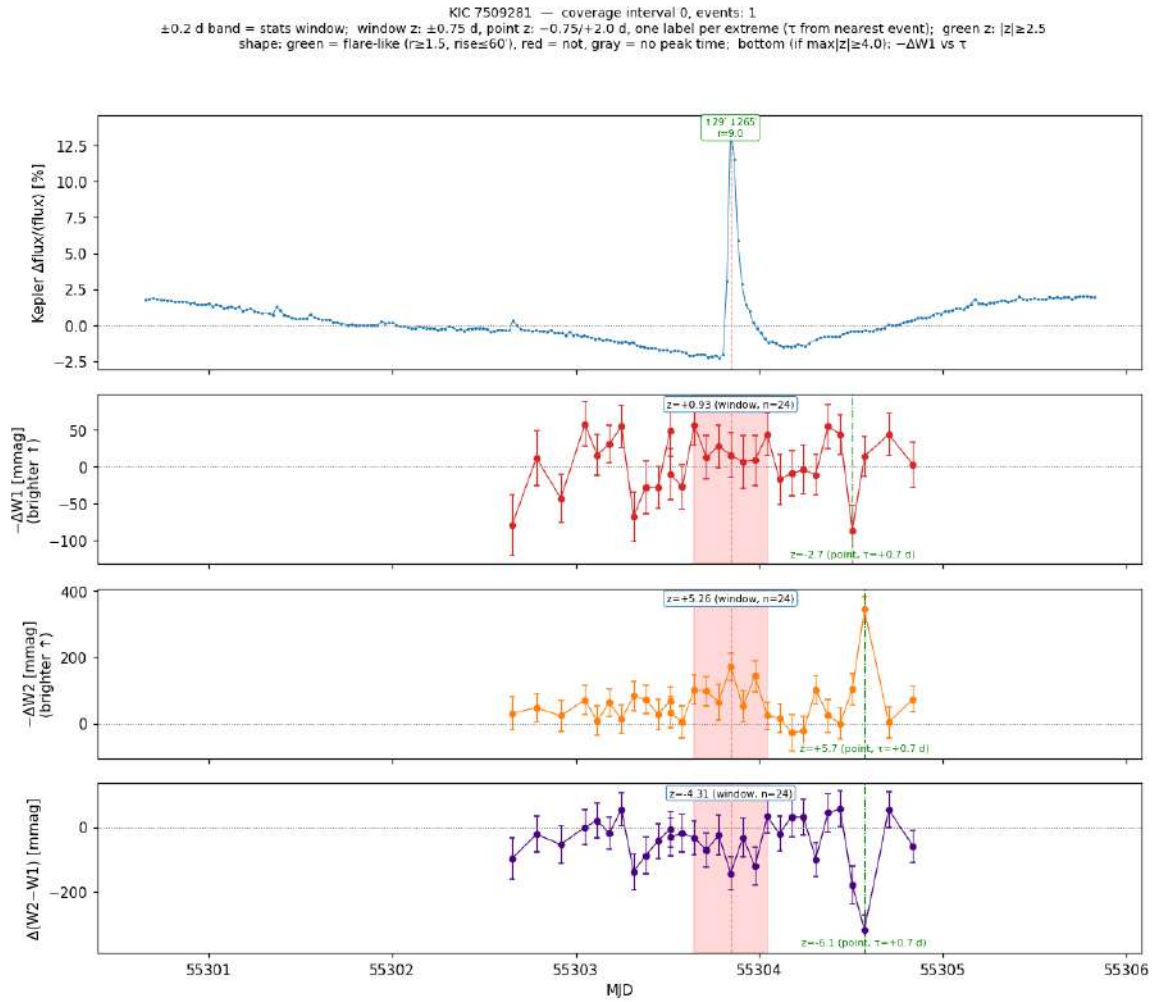

Figure A4: KIC 7509281 (catalogue of Yang & Liu 2019), Kepler at 30-min cadence and AllWISE, series 0: a flare with an amplitude of 13% ($r = 9$). Relative to the level over both AllWISE series the mean deviation over the 24 exposures within ±0.75 d is insignificant in W1 ($z = +0.9$) but appears significant in W2 ($z = +5.3$), with a reddening of the colour. This is not an event but the offset between the cryogenic series shown here (April–May 2010) and the post-cryogenic one (October–November 2010; Section 5): the two series of this star differ by 16 mmag in W1 and 41 mmag in W2, and relative to the median of its own series the W2 mean of the window is +14 mmag ($z \approx 1.5$). The figure illustrates why the Kepler flares are compared only within the series.

Appendix B Formal definition of the quantities

This appendix gives the formal definitions behind Section 3.2. All intervals are input parameters of the program.

Notation. For a star with K catalogued flares let $t_k^{\rm s}$, $t_k^{\rm p}$ and $t_k^{\rm e}$ ($k = 1, \ldots, K$) be the start, peak and end times of flare k. The NEOWISE exposures of the star form V observing series (visits, separated by about half a year); series v contains n_v exposures at times t_{vj} ($j = 1, \ldots, n_v$, spaced by ≈ 95 min) with magnitudes W_{vj}, errors e_{vj} and a quality flag $q_{vj} \in \{0, 1\}$ (1 = clean). The time of exposure (v, j) from the peak of flare k is

$$\tau_{vj}^{(k)} = t_{vj} - t_k^{\rm p}, \tag{B1}$$

where t_{vj} is the time of the exposure and $t_k^{\rm p}$ the time of the peak of flare k; the time from the nearest flare is $\tau_{vj} = \tau_{vj}^{(k^*)}$ with $k^* = \arg\min_k |\tau_{vj}^{(k)}|$. All intervals below are defined in τ and are input parameters of the program.

Quiescent level. The quiescent level of a star in each band and in the colour W2−W1 is determined from the clean exposures outside the vicinity of all its flares,

$$Q = \{(v, j) :\ q_{vj} = 1 \text{ and } \tau_{vj}^{(k)} \notin [-\Delta\tau_-,\ \Delta\tau_+] \text{ for all } k\}, \qquad \Delta\tau_- = 0.85 \text{ d},\ \Delta\tau_+ = 2.1 \text{ d}, \tag{B2}$$

where Q is the set of quiescent exposures of the star, q_{vj} the quality flag defined above, $\tau_{vj}^{(k)}$ the time of the exposure from the peak of flare k, and $\Delta\tau_-$, $\Delta\tau_+$ the half-widths of the exclusion zone before and after a flare, taken somewhat wider than the search interval of Eq. (B6); $N_Q = |Q| = \sum_v n_v^Q$ is the number of quiescent exposures of the star and n_v^Q their number in series v. The level and the scatter are then the robust estimates

$$m = \operatorname*{med}_{(v,j)\in Q} W_{vj}, \qquad \mathrm{MAD} = \operatorname*{med}_{(v,j)\in Q} |W_{vj} - m|, \qquad \sigma = \max\Big(1.4826\,\mathrm{MAD},\ \operatorname*{med}_{(v,j)\in Q} e_{vj}\Big), \tag{B3}$$

where m is the quiescent level of the star in the given band, W_{vj} the magnitude measured in exposure (v, j), MAD the median absolute deviation of these magnitudes from m, e_{vj} the error of a single measurement, and σ the adopted scatter of the quiescent level, for which 1.4826 MAD equals the standard deviation of a Gaussian distribution and the median error serves as a floor. The median and the MAD, unlike the mean and the variance, are insensitive to individual outliers, of which single-exposure photometry contains many. At least $N_Q = 15$ exposures are required — with fewer, the relative error of σ (about $1.1/\sqrt{N_Q}$) exceeds 30%, and the star is excluded from the statistics. The deviation of every exposure and its significance are

$$\Delta_{vj} = m - W_{vj}, \qquad z_{vj} = \Delta_{vj}/\sigma, \tag{B4}$$

where Δ_{vj} is the deviation of exposure (v, j) from the quiescent level, expressed in magnitudes, and z_{vj} the same deviation in units of σ; a positive Δ_{vj} is a brightening. The level of Eq. (B3) is taken over all series of the mission. In doing so one has to allow for a slow, brightness-dependent drift of the NEOWISE single-exposure photometry (known from the data releases; Cutri et al., 2015). For the 13 500 stars of the Seli et al. (2025) sample with clean exposures, the yearly median of the quiescent exposures relative to the median over the whole mission is +8 mmag in 2014, +6 in 2015–2016, +3 in 2017, 0 in 2018, −3 in 2019, −5 to −6 in 2020–2023 and −11 mmag in 2024 in W2, and +1 to +2 mmag in 2014–2017, 0 in 2018, −1 in 2019–2023 and −3.5 mmag in 2024 in W1; the change occurs mainly in 2017–2019, is coherent (91% of the stars are fainter in W2 in 2019–2023 than in 2014–2015), is the same in all intervals of ecliptic latitude, and grows from about 9 mmag between 2014 and 2023 for W1 < 9.5 mag to about 24 mmag for W1 = 11–13 mag. For the search for individual events and for the figures the drift is immaterial: it stays within about ±10 mmag, below the scatter of a single exposure, and shifts z by at most 0.5. For the averaging over hundreds of flares (Section 5) it is not: all TESS flares fall in 2018–2023, so that a comparison of the flare windows with a level over the whole mission turns the drift into a spurious mean "dimming" of -2.0 ± 0.5 mmag in W1 and -6.0 ± 0.4 mmag in W2 for 1439 flares of the Seli et al. (2025) sample in a first run without the quality and saturation selection. The averaging is therefore compared with control windows taken in the same observing series as the flare (Section 5), which cancels the drift; the alternative, a level within the series, $m_v = \mathrm{med}_{j:\,(v,j)\in Q} W_{vj}$, requires $n_v^Q \geq 15$ quiescent exposures in the series and leaves only the stars near the ecliptic poles. Stars brighter than the onset of saturation of the single exposures (W1 ≈ 8.0, W2 ≈ 7.0 mag; Cutri et al. 2015), whose profile-fit photometry carries a time-variable bias, are excluded from the averaging

doi: https://doi.org/10.52526/25792776-26.73.2-227

(not from the search for individual events); without this selection the sample of Section 5 grows to 936 flares of 419 stars and the result is unchanged.

Time intervals. For every flare k two sets of exposures are considered. The averaging window of half-width $\Delta\tau_{\rm A} = 0.2$ d and its mean deviation are

$$A_k = \{(v,j):\ q_{vj}=1,\ |\tau_{vj}^{(k)}| \le \Delta\tau_{\rm A}\}, \qquad n_k = |A_k|, \qquad \bar\Delta_k = \frac{1}{n_k}\sum_{(v,j)\in A_k}\Delta_{vj}, \qquad \bar z_k = \frac{\bar\Delta_k\sqrt{n_k}}{\sigma}, \quad \text{(B5)}$$

where A_k is the set of clean exposures inside the averaging window of flare k, n_k their number, $\bar\Delta_k$ the mean deviation in the window and $\bar z_k$ its significance, the scatter of a mean of n_k exposures being $\sigma/\sqrt{n_k}$. These quantities serve for averaging the deviations over all flares (stacking) and for the upper limits (Section 5). The search interval

$$S_k = \{(v,j):\ q_{vj}=1,\ -\Delta\tau_{\rm S}^{-} \le \tau_{vj}^{(k)} \le \Delta\tau_{\rm S}^{+}\}, \qquad \Delta\tau_{\rm S}^{-} = 0.75\ \text{d},\ \Delta\tau_{\rm S}^{+} = 2.0\ \text{d}, \quad \text{(B6)}$$

where S_k is the set of clean exposures of flare k inside the search interval and $\Delta\tau_{\rm S}^{-}$, $\Delta\tau_{\rm S}^{+}$ are its half-widths before and after the peak. This set serves for the search for individual events: within it the extreme deviations on either side of the peak, $z_k^{-} = \mathrm{extr}\{z_{vj} : \tau_{vj}^{(k)} < 0\}$ and $z_k^{+} = \mathrm{extr}\{z_{vj} : \tau_{vj}^{(k)} > 0\}$ (the value of largest modulus), and the times of the nearest exposures before and after the peak, $\tau_k^{-} = \max\{\tau_{vj}^{(k)} < 0\}$ and $\tau_k^{+} = \min\{\tau_{vj}^{(k)} > 0\}$, are recorded; an exposure falls *during* the flare if $t_k^{\rm s} \le t_{vj} \le t_k^{\rm e}$. The asymmetry of the interval reflects the fact that a response follows the flare and may last from hours to a day (Section 6); the part before the peak is retained to monitor the state of the star before the flare and to reveal events of the opposite sign. A flare is considered to be "in the search interval" if $S_k \neq \varnothing$. For a star with several flares in one series the sets A_k and S_k of different flares may overlap; each exposure is then attributed to the flare nearest in time.

Appendix C Averaging over flares and the upper limit

The window means $\bar\Delta_k$ of Eq. (B5) are combined over the N flares of the cleaned catalogue that pass the quality selection of Section 2 (at least five points and an amplitude of at least five times the scatter), have $n_k \ge 1$ and at least one quiescent exposure in the same observing series; within a window the deviations are clipped at $|\Delta_{vj}| \le 5\sigma$, and stars whose window means are systematically offset (median $|\bar z_k| > 10$, a sign of a corrupted quiescent level) are excluded. Each flare enters with unit weight regardless of n_k and of the star, and the flare-averaged response is the trimmed mean

$$\hat D = \frac{1}{N-2r}\sum_{k=r+1}^{N-r}\bar\Delta_{(k)}, \qquad r = \lfloor 0.1N \rfloor, \quad \text{(C1)}$$

where $\hat D$ is the flare-averaged response, N the number of flares in the sample, $\bar\Delta_{(k)}$ the window means of Eq. (B5) arranged in increasing order and r the number of values discarded at either end (10%) as protection against isolated frame defects. The reference value of $\hat D$ in the absence of a response is not zero, because of the drift of Section 3.2, and is obtained from a null (placebo) construction: in each of $B = 500$ realisations every flare k is assigned a random time $t_k^{(b)}$ drawn from the quiescent exposures Q of the same star in the same observing series (this cancels the drift), the quiescent level is recomputed without the exposures within $[-\Delta\tau_-, \Delta\tau_+]$ of $t_k^{(b)}$, exactly as for a real flare, the same window statistic $\bar e_k^{(b)}$ is computed around $t_k^{(b)}$, and the trimmed mean $\hat D_b$ of these N values is formed; $\mu_0 = \frac{1}{B}\sum_b \hat D_b$. The uncertainty of $\hat D - \mu_0$ is not taken as $\sigma/\sqrt{N}$, because the flares of one star share its quiescent level and, within one series, its exposures; nor can it be taken as the spread of $\{\hat D_b\}$, which, the quiescent exposures of a series being few (a median of 17 for TESS and 13 for Kepler) and the windows overlapping, is 1.5–2.3 times too small. It is obtained instead by a bootstrap over stars: the stars of the sample are drawn with replacement, each with all its flares, the statistic $\hat D - \hat E$ is recomputed, where $\hat E$ is the trimmed mean of the per-flare placebo means $\bar e_k = \frac{1}{B}\sum_b \bar e_k^{(b)}$, and s is the standard deviation of this statistic over 2000 draws. The bootstrap serves only for s: $\hat E$ differs from μ_0 by 0.1–0.5 mmag, because the single-window values are skewed and the trimmed mean is not linear, and the central value is taken as $\hat D - \mu_0$. The one-sided 95% upper limit on a brightening is

$$U_{95} = \max(\hat D - \mu_0,\ 0) + 1.645\, s, \quad \text{(C2)}$$

where U_{95} is the upper limit on a mean brightening, μ_0 the mean of the null realisations $\hat{D}_b$ ($b = 1, \ldots, B$), s the bootstrap uncertainty of $\hat{D} - \mu_0$, and 1.645 the quantile of the normal distribution corresponding to a one-sided 95% confidence level. The significance of the observed value follows from $(\hat{D} - \mu_0)/s$. When $\hat{D} - \mu_0 < 0$ the limit equals $1.645\,s$ and is set by the noise alone. For the colour W2−W1 a positive deviation is a reddening (a relative brightening in W2). The same construction with the exposures of the search interval sorted into bins of τ (the window $|\tau - \tau_b| \le \Delta\tau_b/2$ in place of A_k) gives the flare-averaged response as a function of time from the peak, $\langle\Delta\rangle(\tau_b)$, to be presented in the recalculation announced in Section 5.

References

Aboudarham J., Henoux J. C., 1987, Astron. Astrophys., 174, 270

Akopian A. A., 2021, Communications of BAO, 68, 150, doi:10.52526/25792776-2021.68.2-150

Akopian A. A., 2024, Astrophysics, 67, 487, doi:10.1007/s10511-025-09847-4

Akopian A. A., Sargsyan G. O., 2026, Astrophysics, doi:10.1007/s10511-026-09968-4

Ambartsumian V. A., 1954, Communications of the Byurakan Astrophysical Observatory, 13, 3

Ambartsumian V. A., 1969, Stars, Nebulae, and Galaxies (collected works), p. 283: Flare stars in the Pleiades. Publishing House of the Academy of Sciences of the Armenian SSR, Yerevan

Ambartsumyan V. A., Mirzoyan L. V., Parsamyan E. S., Chavushyan O. S., Erastova L. K., 1970, Astrophysics, 6, 1, doi:10.1007/BF01002566

Astropy Collaboration et al., 2022, Astrophys. J., 935, 167, doi:10.3847/1538-4357/ac7c74

Benz A. O., Güdel M., 2010, Ann. Rev. Astron. Astrophys., 48, 241, doi:10.1146/annurev-astro-082708-101757

Borucki W. J., Koch D., Basri G., et al., 2010, Science, 327, 977, doi:10.1126/science.1185402

Bruno G., Pagano I., Scandariato G., et al., 2024, Astron. Astrophys., 686, A239, doi:10.1051/0004-6361/202348951

Crowley J., Wheatland M. S., Yang K., 2022, Astrophys. J., 941, 193, doi:10.3847/1538-4357/aca476

Cutri R. M., Wright E. L., Conrow T., et al., 2013, Explanatory Supplement to the AllWISE Data Release Products, IPAC/Caltech

Cutri R. M., Mainzer A., Conrow T., et al., 2015, Explanatory Supplement to the NEOWISE Data Release Products, IPAC/Caltech

Davenport J. R. A., 2016, Astrophys. J., 829, 23, doi:10.3847/0004-637X/829/1/23

Davenport J. R. A., Becker A. C., Kowalski A. F., et al., 2012, Astrophys. J., 748, 58, doi:10.1088/0004-637X/748/1/58

Davenport J. R. A., Hawley S. L., Hebb L., et al., 2014, Astrophys. J., 797, 122, doi:10.1088/0004-637X/797/2/122

Davenport J. R. A., Covey K. R., Clarke R. W., et al., 2019, Astrophys. J., 871, 241, doi:10.3847/1538-4357/aafb76

Doyle J. G., Butler C. J., Byrne P. B., van den Oord G. H. J., 1988, Astron. Astrophys., 193, 229

Feinstein A. D., Seligman D. Z., Günther M. N., Adams F. C., 2022, Astrophys. J. Lett., 925, L9, doi:10.3847/2041-8213/ac4b5e

Feinstein A. D., Seligman D. Z., France K., Gagné J., Kowalski A., 2024, Astron. J., 168, 60, doi:10.3847/1538-3881/ad4edf

Gaia Collaboration et al., 2023, Astron. Astrophys., 674, A1, doi:10.1051/0004-6361/202243940

Gershberg R. E., 2005, Solar-Type Activity in Main-Sequence Stars. Springer, Berlin, doi:10.1007/3-540-28243-2

Giampapa M. S., Africano J. L., Klimke A., et al., 1982, Astrophys. J. Lett., 252, L39, doi:10.1086/183715

Ginsburg A., Sipőcz B. M., Brasseur C. E., et al., 2019, Astron. J., 157, 98, doi:10.3847/1538-3881/aafc33

Günther M. N., Zhan Z., Seager S., et al., 2020, Astron. J., 159, 60, doi:10.3847/1538-3881/ab5d3a

Haro G., 1957, in Herbig G. H., ed., IAU Symposium 3, Non-stable Stars. Cambridge University Press, Cambridge, p. 26

Hawley S. L., Fisher G. H., 1992, Astrophys. J. Suppl. Ser., 78, 565, doi:10.1086/191640

Hawley S. L., Davenport J. R. A., Kowalski A. F., et al., 2014, Astrophys. J., 797, 121, doi:10.1088/0004-637X/797/2/121

Henoux J. C., Aboudarham J., Brown J. C., et al., 1990, Astron. Astrophys., 233, 577

Howard W. S., Kowalski A. F., Flagg L., et al., 2023, Astrophys. J., 959, 64, doi:10.3847/1538-4357/acfe75

Howell S. B., Sobeck C., Haas M., et al., 2014, Publ. Astron. Soc. Pac., 126, 398, doi:10.1086/676406

Ilin E., Schmidt S. J., Davenport J. R. A., Strassmeier K. G., 2019, Astron. Astrophys., 622, A133, doi:10.1051/0004-6361/201834400

Ilin E., Schmidt S. J., Poppenhäger K., et al., 2021, Astron. Astrophys., 645, A42, doi:10.1051/0004-6361/202039198

Jackman J. A. G., Shkolnik E. L., Million C., et al., 2023, Mon. Not. R. Astron. Soc., 519, 3564, doi:10.1093/mnras/stac3135

Kowalski A. F., 2024, Living Reviews in Solar Physics, 21, 1, doi:10.1007/s41116-024-00039-4

Kowalski A. F., Hawley S. L., Wisniewski J. P., et al., 2013, Astrophys. J. Suppl. Ser., 207, 15, doi:10.1088/0067-0049/207/1/15

Kowalski A. F., Mathioudakis M., Hawley S. L., et al., 2016, Astrophys. J., 820, 95, doi:10.3847/0004-637X/820/2/95

Kowalski A. F., Allred J. C., Carlsson M., 2024, Astrophys. J., 969, 121, doi:10.3847/1538-4357/ad4148

Leitzinger M., Odert P., Greimel R., et al., 2014, Mon. Not. R. Astron. Soc., 443, 898, doi:10.1093/mnras/stu1161

Lightkurve Collaboration et al., 2018, Lightkurve: Kepler and TESS time series analysis in Python, Astrophysics Source Code Library, ascl:1812.013

Loyd R. O. P., France K., Youngblood A., et al., 2018, Astrophys. J., 867, 71, doi:10.3847/1538-4357/aae2bd

Luger R., Agol E., Kruse E., et al., 2016, Astron. J., 152, 100, doi:10.3847/0004-6256/152/4/100

Maehara H., Shibayama T., Notsu S., et al., 2012, Nature, 485, 478, doi:10.1038/nature11063

Mainzer A., Bauer J., Grav T., et al., 2011, Astrophys. J., 731, 53, doi:10.1088/0004-637X/731/1/53

Mainzer A., Bauer J., Cutri R. M., et al., 2014, Astrophys. J., 792, 30, doi:10.1088/0004-637X/792/1/30

Mamonova E., Kowalski A. F., Herbst K., Wedemeyer S., Werner S. C., 2025, Astron. Astrophys., 705, A165, doi:10.1051/0004-6361/202556844

Oskanian V. S., Terebizh V. Y., 1971, Astrophysics, 7, 48, doi:10.1007/BF01002621

Osten R. A., Wolk S. J., 2015, Astrophys. J., 809, 79, doi:10.1088/0004-637X/809/1/79

Osten R. A., Hawley S. L., Allred J. C., Johns-Krull C. M., Roark C., 2005, Astrophys. J., 621, 398, doi:10.1086/427275

Pratt V., Reeves J. R., Martin D. V., et al., 2026, Astrophys. J., 1001, 171, doi:10.3847/1538-4357/ae5804

Pye J. P., Rosen S., Fyfe D., Schröder A. C., 2015, Astron. Astrophys., 581, A28, doi:10.1051/0004-6361/201526217

Ricker G. R., Winn J. N., Vanderspek R., et al., 2015, Journal of Astronomical Telescopes, Instruments, and Systems, 1, 014003, doi:10.1117/1.JATIS.1.1.014003

Rodonò M., Pucillo M., Sedmak G., de Biase G. A., 1979, Astron. Astrophys., 76, 242

Schmidt S. J., Kowalski A. F., Hawley S. L., Hilton E. J., Wisniewski J. P., Tofflemire B. M., 2012, Astrophys. J., 745, 14, doi:10.1088/0004-637X/745/1/14

Seli B., Vida K., Oláh K., et al., 2025, Astron. Astrophys., 694, A161, doi:10.1051/0004-6361/202452489

Shibayama T., Maehara H., Notsu S., et al., 2013, Astrophys. J. Suppl. Ser., 209, 5, doi:10.1088/0067-0049/209/1/5

Smith J. C., Stumpe M. C., Van Cleve J. E., et al., 2012, Publ. Astron. Soc. Pac., 124, 1000, doi:10.1086/667697

Stassun K. G., Oelkers R. J., Paegert M., et al., 2019, Astron. J., 158, 138, doi:10.3847/1538-3881/ab3467

Stumpe M. C., Smith J. C., Van Cleve J. E., et al., 2012, Publ. Astron. Soc. Pac., 124, 985, doi:10.1086/667698

Tofflemire B. M., Wisniewski J. P., Kowalski A. F., et al., 2012, Astron. J., 143, 12, doi:10.1088/0004-6256/143/1/12

Tovmassian H. M., Zalinian V. P., Silant'ev N. A., Cardona O., Chavez M., 2003, Astron. Astrophys., 399, 647, doi:10.1051/0004-6361:20021754

Ventura R., Peres G., Pagano I., Rodonò M., 1995, Astron. Astrophys., 303, 509

Veronig A. M., Odert P., Leitzinger M., et al., 2021, Nature Astronomy, 5, 697, doi:10.1038/s41550-021-01345-9

Walkowicz L. M., Basri G., Batalha N., et al., 2011, Astron. J., 141, 50, doi:10.1088/0004-6256/141/2/50

Williams J. P., Cieza L. A., 2011, Ann. Rev. Astron. Astrophys., 49, 67, doi:10.1146/annurev-astro-081710-102548

Wright E. L., Eisenhardt P. R. M., Mainzer A. K., et al., 2010, Astron. J., 140, 1868, doi:10.1088/0004-6256/140/6/1868

Wyatt M. C., 2008, Ann. Rev. Astron. Astrophys., 46, 339, doi:10.1146/annurev.astro.45.051806.110525

Yang H., Liu J., 2019, Astrophys. J. Suppl. Ser., 241, 29, doi:10.3847/1538-4365/ab0d28

Yudovich D. G., Yang K. E., Sun X., 2025, Astrophys. J., 984, 186, doi:10.3847/1538-4357/adc695